SCIENCE CHINA
Technological Sciences

December 2011 Vol.54 No.12: 3130–3136
doi: 10.1007/s11431-011-4611-x

Milling stability analysis using the spectral method

DING Ye[1], ZHU LiMin[1], ZHANG XiaoJian[2] & DING Han[1*]

[1] *State Key Laboratory of Mechanical System and Vibration, Shanghai Jiao Tong University, Shanghai 200240, China;*
[2] *State Key Laboratory of Digital Manufacturing Equipment and Technology, Huazhong University of Science and Technology, Wuhan 430074, China*

Received August 24, 2011; accepted September 13, 2011; published online November 5, 2011

This paper focuses on the development of an efficient semi-analytical solution of chatter stability in milling based on the spectral method for integral equations. The time-periodic dynamics of the milling process taking the regenerative effect into account is formulated as a delayed differential equation with time-periodic coefficients, and then reformulated as a form of integral equation. On the basis of one tooth period being divided into a series of subintervals, the barycentric Lagrange interpolation polynomials are employed to approximate the state term and the delay term in the integral equation, respectively, while the Gaussian quadrature method is utilized to approximate the integral term. Thereafter, the Floquet transition matrix within the tooth period is constructed to predict the chatter stability according to Floquet theory. Experimental-validated one-degree-of-freedom and two-degree-of-freedom milling examples are used to verify the proposed algorithm, and compared with existing algorithms, it has the advantages of high rate of convergence and high computational efficiency.

milling stability, delayed differential equation, integral equation, spectral method, Floquet theory

Citation: Ding Y, Zhu L M, Zhang X J, et al. Milling stability analysis using the spectral method. Sci China Tech Sci, 2011, 54: 3130–3136, doi: 10.1007/s11431-011-4611-x

1 Introduction

High-speed milling is one of the most important basic technologies for machining high precision complex surfaces widely utilized in key industries, e.g., aerospace, automotive, shipping, die and mold. It has some well-known advantages, such as obtaining a large material removal rate, keeping relatively low cutting forces and maintaining a high quality level. However, chatter is one of the most severe limitations for surface quality and productivity in milling operations due to choosing improper machining parameters. To achieve the aim of high performance milling [1–3], a great deal of effort have been dedicated to improvment of production efficiency and part quality in milling through modeling the dynamic milling processes and avoiding chatter by selecting optimal cutting parameters. In general, there are four kinds of chatter mechanisms [4] in metal cutting, i.e., frictional chatter, regenerative chatter, mode-coupling chatter and thermo-mechanical chatter. In milling operations, the regenerative chatter is the most common form of self-excited and unstable vibrations. The dynamic milling process taking the regenerative effect into account is generally formulated as a delayed differential equation (DDE) with time-periodic coefficients [5–7].

Based on the DDE, stability analysis for dynamic milling processes with different machining parameters is one of the most important prerequisites for the high speed milling technology. The time-domain simulation methods [8–11] can provide powerful predictions of stability limits simultaneously considering some non-linearities such as the loss of contact effect and radial immersion varying due to deflection, however, the computational burden is undesirably high.

*Corresponding author (email: hding@sjtu.edu.cn)

To reduce the computational burden yet hold with reasonable numerical accuracy, many semi-analytical methods have been investigated for the last two decades. Altintas et al. proposed the single frequency method [12] and the multi frequency solution [13, 14], which can work in the cases of three dimensional milling [15], plunge milling [16], circular milling [17], five-axis ball-end milling [18], etc. Bayly and his colleagues developed the temporal finite element analysis (TFEA) method [19], which can be generalized to the non-linear TFEA formulation [20] and prediction of the surface location error in milling [21, 22]. Insperger and Stépán explored the semi-discretization method (SDM) [23, 24], and the first-order SDM [25], which are widely used in many cases, such as stability analysis for up-milling and down-milling [26, 27], stability prediction for milling processes with variable time delays [28], in consideration of the loss-of-contact and feed-rate effects [29], milling with variable pitch and variable helix milling tools [30], milling with spindle speed variation [31], etc. Wan et al. [32] recently proposed an improved semi-discretization method for predicting the chatter stability of milling processes considering multiple delays, i.e., the effects of runout and variable pitch of tools. Olgac and Sipahi [33] suggested the method of cluster treatment of characteristic roots (CTCR). Butcher and his co-workers [34] presented the Chebyshev polynomial based method and the Chebyshev collocation method [35]. We introduced the full-discretization method (FDM) [36] based on the direct integration scheme, which can be used for simultaneous prediction of the surface location error in milling [37]. Insperger [38] then gave another formulation of the FDM from the viewpoint of differential equations.

More recently, we proposed the numerical integration method [39] for prediction of milling stability by using the numerical techniques of integral equations. In ref. [39], the original DDE is firstly represented as an integral equation with time delays, and then the classical numerical integration method (Nystroem method) for Volterra equations of the second kind (without time delays) are generalized to establish the Floquet transition matrix over one tooth passing period. The rate of convergence of the numerical integration method is limited [39] since only two (or three) discretized state and time-delay terms are employed for interpolation over each subinterval of one time period during the procedure of constructing the Floquet transition matrix,. In this paper, to improve the rate of convergence and the numerical performance of our preliminary work [40] only applicable to the case of low radial immersion milling, a spectral method suitable for cases of high radial immersion milling and low radial immersion milling is presented to establish the approximate Floquet transition matrix for prediction of chatter stability, motivated by the spectral method [41, 42] for Volterra integral equations of the second kind. The remarkable property of the spectral method is that the spectral accuracy (or the exponential rate of convergence) can be obtained. When revising this paper, we were aware of the work of Khasawneh and Mann [43] which also proposed the spectral method for stability of DDEs. However, the basic principles are different. In ref. [43] the spectral method was presented in the framework of the method of weighted residuals, while in this paper the algorithm is constructed on the basis of the spectral method [41, 42] for Volterra integral equations.

The remainder of this paper is organized as follows. In Section 2, the formulation of the dynamic milling process taking the regenerative effect into account is briefly introduced. In Section 3, the spectral method for milling stability analysis is presented. In Section 4, two kinds of general milling models, i.e., one-degree-of-freedom and two-degree-of-freedom milling examples which have been experimentally validated, are used to verify the proposed algorithm. Conclusions are drawn in Section 5.

2 Mathematical model

Without loss of generality, the dynamic milling process taking the regenerative effect into account is generally modeled as a m-dimensional time-periodic system with a single discrete time delay in the following state-space form:

$$\dot{\boldsymbol{x}}(t) = \boldsymbol{A}\boldsymbol{x}(t) + a_p\boldsymbol{B}(t)\left[\boldsymbol{x}(t) - \boldsymbol{x}(t-T)\right], \tag{1}$$

where a_p denotes the axial depth of cut, $\boldsymbol{A}$ is a constant matrix representing the time-invariant nature of the system, $\boldsymbol{B}(t)$ is a periodic-coefficient matrix due to the time-variant cutting forces, i.e., $\boldsymbol{B}(t) = \boldsymbol{B}(t+T)$, and T is the time delay which is equal to the time period.

For more detailed descriptions of the dynamic milling process, the readers can refer to refs. [5, 6].

3 Algorithm of calculation

Denoting by t_0 and t_f the time the cutting tool leaves the workpiece and the duration of the free vibration, the forced vibration duration $t_c=(T-t_f)$. The forced vibration duration is then discretized as n subintervals, and we denote the discretized time points in cutting by t_i, $i=1,\ldots,n+1$, where $t_1=t_0+t_f$ and $t_{n+1}=t_0+T$. In this paper, the set of $(n+1)$ Chebyshev points of the second kind [44] is employed to space the time nodes t_i, $i=1,\ldots,n+1$ in the forced vibration duration, i.e.,

$$t_i = \frac{t_1+t_{n+1}}{2} - \frac{t_{n+1}-t_1}{2}\cos\left(\frac{(i-1)\pi}{n}\right), i=1,\ldots,n+1. \tag{2}$$

Eq. (1) can be represented as the following integral equation:

$$\begin{aligned}\boldsymbol{x}(t) &= \mathrm{e}^{\boldsymbol{A}(t-t_0)}\boldsymbol{x}(t_0)\\ &\quad + a_p\int_{t_0}^{t}\left\{\mathrm{e}^{\boldsymbol{A}(t-\xi)}\boldsymbol{B}(\xi)\left[\boldsymbol{x}(\xi)-\boldsymbol{x}(\xi-T)\right]\right\}\mathrm{d}\xi,\end{aligned} \tag{3}$$

where $\boldsymbol{x}(t_0)$ denotes the state value at t=t_0.

At the end of the free vibration duration, the response of the system at t_1 can be deduced from eq. (3) as

$$\boldsymbol{x}(t_1)=\boldsymbol{x}(t_0+t_f)=\mathrm{e}^{At_f}\boldsymbol{x}(t_0). \tag{4}$$

As for $t\geqslant t_1$, the response is

$$\begin{aligned}\boldsymbol{x}(t)&=\mathrm{e}^{A(t-t_1)}\boldsymbol{x}(t_1)\\&+a_p\int_{t_1}^{t}\left\{\mathrm{e}^{A(t-\xi)}\boldsymbol{B}(\xi)\boldsymbol{x}(\xi)\right\}\mathrm{d}\xi\\&-a_p\int_{t_1}^{t}\left\{\mathrm{e}^{A(t-\xi)}\boldsymbol{B}(\xi)\boldsymbol{x}(\xi-T)\right\}\mathrm{d}\xi.\end{aligned} \tag{5}$$

At the discretized time nodes t_i, i = 2,…, n+1, the corresponding responses can be obtained from eq. (5) as

$$\begin{aligned}\boldsymbol{x}(t_i)&=\mathrm{e}^{A(t_i-t_1)}\boldsymbol{x}(t_1)\\&+a_p\int_{t_1}^{t_i}\left\{\mathrm{e}^{A(t_i-\xi)}\boldsymbol{B}(\xi)\boldsymbol{x}(\xi)\right\}\mathrm{d}\xi\\&-a_p\int_{t_1}^{t_i}\left\{\mathrm{e}^{A(t_i-\xi)}\boldsymbol{B}(\xi)\boldsymbol{x}(\xi-T)\right\}\mathrm{d}\xi.\end{aligned} \tag{6}$$

Following ref. [41], a linear transformation is introduced for the definite integral term in eq. (6), i.e.,

$$\xi(t_i,\varepsilon)=\frac{t_i-t_1}{2}\varepsilon+\frac{t_i+t_1}{2}. \tag{7}$$

Then, eq. (6) is re-expressed as

$$\begin{aligned}\boldsymbol{x}(t_i)&=\mathrm{e}^{A(t_i-t_1)}\boldsymbol{x}(t_1)\\&+a_p\frac{t_i-t_1}{2}\int_{-1}^{1}\left\{\mathrm{e}^{A[t_i-\xi(t_i,\varepsilon)]}\boldsymbol{B}\big(\xi(t_i,\varepsilon)\big)\boldsymbol{x}\big(\xi(t_i,\varepsilon)\big)\right\}\mathrm{d}\varepsilon\\&-a_p\frac{t_i-t_1}{2}\int_{-1}^{1}\left\{\mathrm{e}^{A[t_i-\xi(t_i,\varepsilon)]}\boldsymbol{B}\big(\xi(t_i,\varepsilon)\big)\boldsymbol{x}\big(\xi(t_i,\varepsilon)-T\big)\right\}\mathrm{d}\varepsilon.\end{aligned} \tag{8}$$

Using the (n+1)-point Gauss-Legendre formula [45], eq. (8) can be reduced to

$$\begin{aligned}\boldsymbol{x}(t_i)&=\mathrm{e}^{A(t_i-t_1)}\boldsymbol{x}(t_1)\\&+a_p\frac{t_i-t_1}{2}\sum_{k=1}^{n+1}\left\{\mathrm{e}^{A[t_i-\xi(t_i,\varepsilon_k)]}\boldsymbol{B}\big(\xi(t_i,\varepsilon_k)\big)\boldsymbol{x}\big(\xi(t_i,\varepsilon_k)\big)\right\}\cdot w_k\\&-a_p\frac{t_i-t_1}{2}\sum_{k=1}^{n+1}\left\{\mathrm{e}^{A[t_i-\xi(t_i,\varepsilon_k)]}\boldsymbol{B}\big(\xi(t_i,\varepsilon_k)\big)\boldsymbol{x}\big(\xi(t_i,\varepsilon_k)-T\big)\right\}\cdot w_k,\end{aligned} \tag{9}$$

where ε_k's are the grid points of the (n+1)-point Gauss-Legendre formula on the interval [−1, 1], and w_k's are the corresponding weights.

To approximate eq. (9), the key point is to calculate the state term $\boldsymbol{x}\big(\xi(t_i,\varepsilon_k)\big)$ and the time delay term $\boldsymbol{x}\big(\xi(t_i,\varepsilon_k)-T\big)$. The barycentric Lagrange interpolation method [46] is employed here to interpolate them by using $\boldsymbol{x}(t_i),\big(i=1,\ldots,n+1\big)$ and $\boldsymbol{x}(t_i-T),\big(i=1,\ldots,n+1\big)$, respectively. The discretized time points t_i, $\big(i=1,\ldots,n+1\big)$ and t_i-T, $\big(i=1,\ldots,n+1\big)$ are actually two sets of nodal coordinates in one dimension. For the sake of clarity, the barycentric Lagrange interpolation method is cited in the **Appendix**. The state term $\boldsymbol{x}(t)$ for $t_1\leqslant t\leqslant t_{n+1}$ can be interpolated as

$$\tilde{\boldsymbol{x}}(t)=\sum_{\ell=1}^{n+1}\big[\varPhi_\ell(t)\cdot\boldsymbol{x}(t_\ell)\big], \tag{10}$$

where $\varPhi_\ell(t),\ell=1,\ldots,n+1$ are the shape functions due to the barycentric Lagrange interpolation. Thereafter, $\boldsymbol{x}\big(\xi(t_i,\varepsilon_k)\big)$ in eq. (9) is approximated as $\tilde{\boldsymbol{x}}\big(\xi(t_i,\varepsilon_k)\big)$.

Similarly, the delay term $\boldsymbol{x}(t-T)$ for $t_1\leqslant t\leqslant t_{n+1}$ can be approximated by $\boldsymbol{x}(t_i-T),i=1,\ldots,n+1$ via the following approximants:

$$\tilde{\boldsymbol{x}}(t-T)=\sum_{\ell=1}^{n+1}\big[\varPhi_\ell(t-T)\cdot\boldsymbol{x}(t_\ell-T)\big]. \tag{11}$$

Then, $\boldsymbol{x}\big(\xi(t_i,\varepsilon_k)-T\big)$ can be approximately obtained as $\tilde{\boldsymbol{x}}\big(\xi(t_i,\varepsilon_k)-T\big)$. Note that the evaluations of the shape functions at different integration points are dependent on the relative locations of the integration points with respect to the background nodal coordinates. Hence, we have $\varPhi_\ell(t)=\varPhi_\ell(t-T)$ for $\ell=1,\ldots,n+1$ and $t_1\leqslant t\leqslant t_{n+1}$.

Substituting $\tilde{\boldsymbol{x}}\big(\xi(t_i,\varepsilon_k)\big)$ and $\tilde{\boldsymbol{x}}\big(\xi(t_i,\varepsilon_k)-T\big)$ into eq. (9), we can obtain $\boldsymbol{x}(t_i)$ for (i = 2,…, n+1) as

$$\begin{aligned}&\boldsymbol{x}(t_i)=\mathrm{e}^{A(t_i-t_1)}\boldsymbol{x}(t_1)\\&+a_p\frac{t_i-t_1}{2}\sum_{\ell=1}^{n+1}\left\{\sum_{k=1}^{n+1}\Big[\mathrm{e}^{A[t_i-\xi(t_i,\varepsilon_k)]}\boldsymbol{B}\big(\xi(t_i,\varepsilon_k)\big)\varPhi_\ell\big(\xi(t_i,\varepsilon_k)\big)\Big]\cdot w_k\right\}\\&\cdot\boldsymbol{x}(t_\ell)\\&-a_p\frac{t_i-t_1}{2}\sum_{\ell=1}^{n+1}\left\{\sum_{k=1}^{n+1}\Big[\mathrm{e}^{A[t_i-\xi(t_i,\varepsilon_k)]}\boldsymbol{B}\big(\xi(t_i,\varepsilon_k)\big)\varPhi_\ell\big(\xi(t_i,\varepsilon_k)\big)\Big]\cdot w_k\right\}\\&\cdot\boldsymbol{x}(t_\ell-T).\end{aligned} \tag{12}$$

Combining eqs. (4) and (12), the transition map between $\boldsymbol{x}(t_i),i=1,\ldots,n+1$ and $\boldsymbol{x}(t_i-T),i=1,\ldots,n+1$ can be established as

$$\big(\boldsymbol{I}-\boldsymbol{F}-a_p\boldsymbol{D}\big)\begin{bmatrix}\boldsymbol{x}(t_1)\\\vdots\\\boldsymbol{x}(t_{n+1})\end{bmatrix}=\big(-a_p\boldsymbol{D}+\boldsymbol{E}\big)\begin{bmatrix}\boldsymbol{x}(t_1-T)\\\vdots\\\boldsymbol{x}(t_{n+1}-T)\end{bmatrix}, \tag{13}$$

where $\boldsymbol{F}=\begin{bmatrix}\boldsymbol{0}&\boldsymbol{0}&\cdots&\boldsymbol{0}&\boldsymbol{0}\\\mathrm{e}^{A(t_2-t_1)}&\boldsymbol{0}&\cdots&\boldsymbol{0}&\boldsymbol{0}\\\mathrm{e}^{A(t_3-t_1)}&\boldsymbol{0}&\ddots&\vdots&\vdots\\\vdots&\vdots&\ddots&\boldsymbol{0}&\boldsymbol{0}\\\mathrm{e}^{A(t_{n+1}-t_1)}&\boldsymbol{0}&\cdots&\boldsymbol{0}&\boldsymbol{0}\end{bmatrix}$, $\boldsymbol{E}=\begin{bmatrix}\boldsymbol{0}&\cdots&\boldsymbol{0}&\mathrm{e}^{At_f}\\\boldsymbol{0}&\cdots&\boldsymbol{0}&\boldsymbol{0}\\\vdots&\ddots&\vdots&\vdots\\\boldsymbol{0}&\cdots&\boldsymbol{0}&\boldsymbol{0}\end{bmatrix}$,

and $\boldsymbol{D}=[D_{i\ell}]$, ($i=1,\ldots,n+1$, $\ell=1,\ldots,n+1$), where $D_{i\ell}$ is block matrix with the following structures:

1) for $i=1$, $\ell=1,\ldots,n+1$, $D_{i\ell}=\boldsymbol{0}$,

2) for $i=2,\ldots,n+1$, $\ell=1,\ldots,n+1$,

$$D_{i\ell}=\frac{t_i-t_1}{2}\cdot\sum_{k=1}^{n+1}\left[\mathrm{e}^{\boldsymbol{A}[t_i-\xi(t_i,\varepsilon_k)]}\boldsymbol{B}\left(\xi(t_i,\varepsilon_k)\right)\Phi_\ell\left(\xi(t_i,\varepsilon_k)\right)\right]\cdot w_k.$$

From eq. (13), the approximate Floquet transition matrix is constructed as

$$\boldsymbol{\Psi}=\left(\boldsymbol{I}-\boldsymbol{F}-a_p\boldsymbol{D}\right)^{-1}\left(-a_p\boldsymbol{D}+\boldsymbol{E}\right). \tag{14}$$

At last, the Floquet theory [47] can be used to determine the stability of the system according to eq. (14). The stability of the system can be determined by using all the eigenvalues of the transition matrix $\boldsymbol{\Psi}$ in modulus, i.e.,

$$\max\left(\left|\lambda\left(\boldsymbol{\Psi}\right)\right|\right)\begin{cases}<1 & \text{stable,}\\ =1 & \text{stability boundary,}\\ >1 & \text{instable.}\end{cases} \tag{15}$$

4 Verification and numerical results

The computer programs of the proposed algorithm are all implemented in MATLAB 7.X and run on a personal computer [Intel Core (TM) 2 Duo Processor, 2.1 GHz, 1 GB]. The experimental-validated one-degree-of-freedom [20, 26, 27] and two-degree-of-freedom [21] milling examples are used to verify the proposed algorithm.

4.1 Example of one-degree-of-freedom milling

The state-space form of the one-degree-of-freedom milling model can be represented as [20, 26, 27]

$$\dot{\boldsymbol{x}}(t)=\boldsymbol{A}\boldsymbol{x}(t)+a_p\boldsymbol{B}(t)\left[\boldsymbol{x}(t)-\boldsymbol{x}(t-T)\right], \tag{16}$$

where

$$\boldsymbol{A}=\begin{bmatrix}-\zeta\omega_n & \dfrac{1}{m_t}\\ m_t\left(\zeta\omega_n\right)^2-m_t\omega_n^2 & -\zeta\omega_n\end{bmatrix},\ \boldsymbol{B}(t)=\begin{bmatrix}0 & 0\\ -h(t) & 0\end{bmatrix}. \tag{17}$$

$h(t)$ is the cutting force coefficient function:

$$h(t)=\sum_{j=1}^{N}g\left(\phi_j(t)\right)\sin\left(\phi_j(t)\right)\left[K_t\cos\left(\phi_j(t)\right)+K_n\sin\left(\phi_j(t)\right)\right], \tag{18}$$

where K_t and K_n are the tangential and the normal linearized cutting force coefficients, respectively, and $\phi_j(t)$ is the angular position of the jth tooth defined by

$$\phi_j(t)=(2\pi\Omega/60)t+(j-1)\cdot 2\pi/N, \tag{19}$$

where N is the number of the cutter teeth and Ω is the spindle speed in revolutions per minute (rpm).

The function $g(\phi_j(t))$ is defined as

$$g\left(\phi_j(t)\right)=\begin{cases}1 & \text{if } \phi_{\mathrm{st}}<\phi_j(t)\bmod 2\pi<\phi_{\mathrm{ex}},\\ 0 & \text{otherwise,}\end{cases} \tag{20}$$

where ϕ_{st} and ϕ_{ex} are the start and exit angles of the jth cutter tooth.

To provide comparison for the computational time and accuracy, stability lobe diagrams are calculated by using the semi-discretization method (SDM) [24] and the proposed method. The system parameters are from refs. [20, 26, 27]: a single fluted cutter, the natural frequency $f_n=\omega_n/(2\pi)=146.5$ Hz, the relative damping is $\zeta=0.0032$, the modal mass is $m_t=2.573$ kg, the cutting force coefficients are $K_t=5.5\times10^8$ N/m^2 and $K_n=2.0\times10^8$ N/m^2. The radial immersion ratio is $a/D=0.237$, where a is the radial depth of cut, D the diameter of the cutter. The original Matlab program of SDM [24] is utilized with the number of discretization intervals over one period as 40. The computational parameter n is chosen as 5 for the proposed method. The 400×200 sized grid of parameters of the spindle speed and depth of cut are both adopted for the two methods. The stability lobe diagrams by using the proposed method and the SDM are shown in Figure 1 for up-milling and down-milling, respectively. It is shown that good agreement is achieved. The elapsed time of the proposed algorithm for each case is about 30 s, while about 1300 s are needed for the SDM. It should be noted that the original SDM program [24] is used here, and its computational efficiency can be improved by some numerical techniques [48].

To demonstrate the rate of convergence of the proposed method, the zeroth-order SDM [24], the first-order SDM [25] and the trapezoidal rule based numerical integration method (NIM) [39] are employed as the benchmark. The local discretization errors for the zeroth-order SDM [24], the first-order SDM [25] and the trapezoidal rule based NIM [39] are $\mathcal{O}(\tau^2)$, $\mathcal{O}(\tau^3)$ and $\mathcal{O}(\tau^3)$, respectively. To compare the computational results more reasonably, the system parameters are chosen from ref. [38]: a two fluted cutter, the natural frequency $f_n=w_n/(2\pi)=922$ Hz, the relative damping is $\zeta=0.011$, the modal mass is $m_t=0.03993$ kg, the cutting force coefficients are $K_t=6\times10^8$ N/m^2 and $K_n=2\times10^8$ N/m^2. Figure 2 illustrates the convergences of the eigenvalues with different computational parameters n for the three different methods, where the radial depth of cut ratio is fixed as the high radial immersion $a/D=1$, and the spindle speed $\Omega=5000$ rpm for down-milling. The axial depth of cuts are chosen as $a_p=1.0$ mm and 0.2 mm, respectively. For reference, the exact eigenvalue $|\mu_0|$ is calculated by the proposed method with the number of discretization intervals over one period as 60. The result shows that the proposed method has a much better rate of convergence than those of

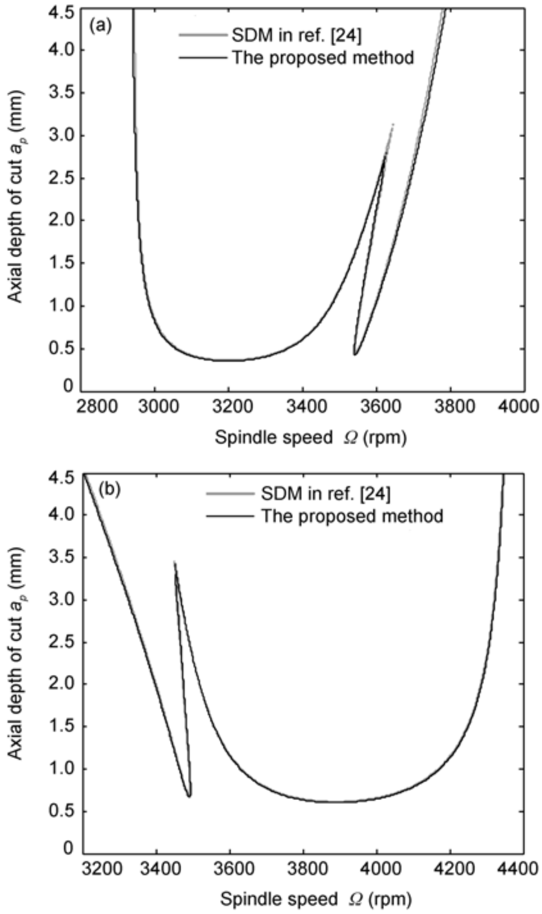

Figure 1 Stability lobe diagrams via the proposed method and the semi-discretization method (SDM): (a) Up-milling; (b) down-milling.

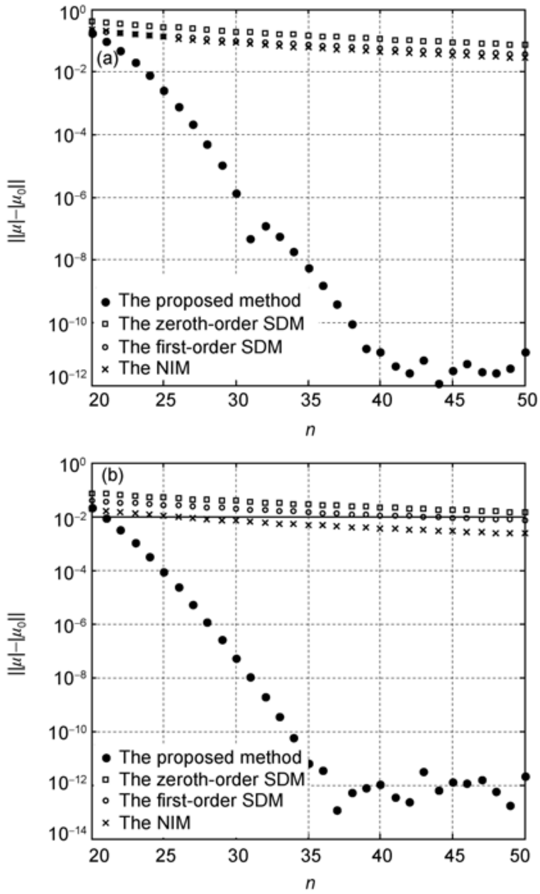

Figure 2 Convergences of the eigenvalues with different computational parameters n for the proposed method, the zeroth-order SDM [24], the first-order SDM [25] and the trapezoidal rule based numerical integration method (NIM) [39]: (a) a_p=1.0 mm, $|\mu_0|$=1.406473528 (unstable); (b) a_p= 0.2 mm, $|\mu_0|$=0.8197427841 (stable).

the others. It should be noted that although the rate of convergence of the trapezoidal rule based NIM [39] is lower than the proposed method, the computational efficiency of NIM is much better than that of the proposed method due to the reason that only sparse matrices are involved in the computational procedure.

4.2 Example of two-degree-of-freedom milling

According to ref. [21], the two-degree-of-freedom milling model is expressed as

$$\dot{\boldsymbol{x}}(t) = \boldsymbol{A}\boldsymbol{x}(t) + a_p \boldsymbol{B}(t)\left[\boldsymbol{x}(t) - \boldsymbol{x}(t-T)\right], \tag{21}$$

where

$$\boldsymbol{A} = \begin{bmatrix} -\boldsymbol{M}^{-1}\boldsymbol{C}/2 & \boldsymbol{M}^{-1} \\ \boldsymbol{C}\boldsymbol{M}^{-1}\boldsymbol{C}/4 - \boldsymbol{K} & -\boldsymbol{C}\boldsymbol{M}^{-1}/2 \end{bmatrix},$$

$$\boldsymbol{B}(t) = \begin{bmatrix} 0 & 0 & 0 & 0 \\ 0 & 0 & 0 & 0 \\ -h_{xx}(t) & -h_{xy}(t) & 0 & 0 \\ -h_{yx}(t) & -h_{yy}(t) & 0 & 0 \end{bmatrix},$$

$\boldsymbol{M}$, $\boldsymbol{C}$, $\boldsymbol{K}$ denote the modal mass, damping and stiffness matrices, respectively, $h_{xx}(t)$, $h_{xy}(t)$, $h_{yx}(t)$ and $h_{yy}(t)$ are the cutting force coefficients defined as

$$h_{xx}(t) = \sum_{j=1}^{N} g\left(\phi_j(t)\right)\sin\left(\phi_j(t)\right)\left[K_t\cos\left(\phi_j(t)\right) + K_n\sin\left(\phi_j(t)\right)\right], \tag{22}$$

$$h_{xy}(t) = \sum_{j=1}^{N} g\left(\phi_j(t)\right)\cos\left(\phi_j(t)\right)\left[K_t\cos\left(\phi_j(t)\right) + K_n\sin\left(\phi_j(t)\right)\right], \tag{23}$$

$$h_{yx}(t) = \sum_{j=1}^{N} g\left(\phi_j(t)\right)\sin\left(\phi_j(t)\right)\left[-K_t\sin\left(\phi_j(t)\right) + K_n\cos\left(\phi_j(t)\right)\right], \tag{24}$$

$$h_{yy}(t) = \sum_{j=1}^{N} g\left(\phi_j(t)\right)\cos\left(\phi_j(t)\right)\left[-K_t\sin\left(\phi_j(t)\right) + K_n\cos\left(\phi_j(t)\right)\right]. \tag{25}$$

In this example, the technological parameters are from ref. [21]: a two fluted cutter, the cutter diameter 12.75 mm, 5% radial immersion down-milling. The cutting coefficient values for the aluminum (7050-T7451) material are K_t=

5.36×10^8 N/m^2 and K_n=1.87×10^8 N/m^2. The cutter modal parameters are cited in Table 1. The TFEA method [21] which has been well validated by experiments is utilized to verify the proposed method. The 200×100 sized grid of parameters of the spindle speed and depth of cut are both adopted for the two methods, and the computational parameter are both chosen as $n = 4$ (for TFEA method, it is the number of elements in cutting). Figure 3 illustrates the comparative results of the two methods, and good agreement is also achieved. In addition, it only takes 13.2 s for the proposed method, while 858.3 s are needed for the TFEA method due to the use of the symbolic calculations in MATLAB. Note that the computational burden for the TFEA method can be reduced if some numerical methods are employed.

5 Conclusion and future work

In this work, an efficient semi-analytical method for milling stability analysis in the framework of integral equations is introduced. Based on the proposed spectral method, the original DDE governing the time-periodic dynamics of the milling process taking the regenerative effect into account is approximated by a set of algebraic equations. On this basis, the Floquet transition matrix is constructed to predict the chatter stability of the system via Floquet theory. The benchmark examples, i.e., one-degree-of-freedom and two-degree-of-freedom milling models, which have been well experimentally validated, are utilized to verify the proposed method. The comparative results illustrate that high-efficiency and high-accuracy are both achieved.

Table 1 The cutter modal parameters from ref. [21]

M (kg)	***C*** (Ns/m)	***K*** (N/m)
$\begin{bmatrix} 0.0436 & 0 \\ 0 & 0.0478 \end{bmatrix}$	$\begin{bmatrix} 4.268 & 0 \\ 0 & 4.355 \end{bmatrix}$	$\begin{bmatrix} 9.14\times10^5 & 0 \\ 0 & 1.00\times10^6 \end{bmatrix}$

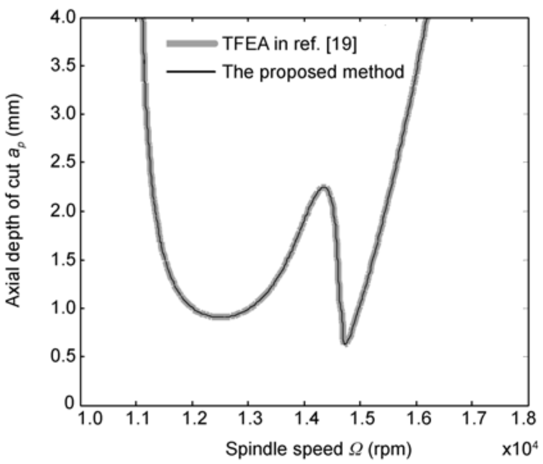

Figure 3 Stability lobe diagrams for the proposed method and the TFEA method.

The present work focuses on the topic of milling stability prediction with applications to the three-axis end-milling. Future works are worth considering. The most important one is to combine the proposed method with some advanced tool path planning methods, such as the third-order point contact approach [49, 50] and the kinematics constrained tool path planning method [51], for five-axis milling process optimization. The second one is to fuse the proposed method with some on-line chatter detection and signal analysis techniques [52, 53] for high performance machining.

Appendix The barycentric Lagrange interpolation [46]

For the Chebyshev time points t_i, $(i=1,\ldots,n+1)$, the state term $\boldsymbol{x}(t)$ for $t_1 \leqslant t \leqslant t_{n+1}$ can be interpolated as

$$\tilde{\boldsymbol{x}}(t)=\sum_{\ell=1}^{n+1}\left[\Phi_\ell(t)\cdot\boldsymbol{x}(t_\ell)\right], \tag{A1}$$

where $\Phi_\ell(t)$,$(i=1,\ldots,n+1)$ is defined as follows:

if $t\neq t_i$ for $i=1,\ldots,n+1$

$$\Phi_\ell(t)=\frac{\dfrac{c_\ell}{t-t_\ell}}{\displaystyle\sum_{i=1}^{n+1}\frac{c_i}{t-t_i}}, \tag{A2}$$

where c_i for the Chebyshev points of the second kind are defined by

$$c_i=(-1)^{i-1}\delta_i,\quad \delta_i=\begin{cases}1/2, & i=1 \text{ or } i=n+1,\\ 1, & \text{otherwise;}\end{cases} \tag{A3}$$

if $t=t_i$ and $i\in\{1,\ldots,n+1\}$

$$\Phi_\ell(t)=\begin{cases}1, & \ell=i,\\ 0, & \text{otherwise.}\end{cases} \tag{A4}$$

This work was partially supported by the National Key Basic Research Program (Grant No. 2011CB706804) and the Science & Technology Commission of Shanghai Municipality (Grant Nos. 09QH1401500 and 10JC1408000).

1 Budak E. Analytical models for high performance milling. Part I: Cutting forces, structural deformations and tolerance integrity. Int J Mach Tools Manuf, 2006, 46(12-13): 1478–1488

2 Budak E. Analytical models for high performance milling. Part II: Process dynamics and stability. Int J Mach Tools Manuf, 2006, 46(12-13): 1489v1499

3 Altintas Y, Merdol S D. Virtual high performance milling. CIRP Ann-Manuf Technol, 2007, 56(1): 81–84

4 Wiercigroch M, Budak E. Sources of nonlinearities, chatter generation and suppression in metal cutting. Philos Trans R Soc A-Math Phys Eng Sci, 2001, 359(1781): 663–693

5 Altintas Y. Manufacturing Automation: Metal Cutting Mechanics, Machine Tool Vibrations, and Cnc Design. Cambridge: Cambridge University Press, 2000

6 Altintas Y, Weck M. Chatter stability of metal cutting and grinding. CIRP Ann-Manuf Technol, 2004, 53(2): 619–642

7 Altintas Y, Stépán G, Merdol D, et al. Chatter stability of milling in frequency and discrete time domain. CIRP J Manuf Sci Technol, 2008, 1(1): 35–44

8 Tlusty J, Ismail F. Basic non-linearity in machining chatter. CIRP Ann-Manuf Technol, 1981, 30(1): 299–304

9 Smith S, Tlusty J. Efficient simulation programs for chatter in milling. CIRP Ann-Manuf Technol, 1993, 42(1): 463–466

10 Campomanes M L, Altintas Y. An improved time domain simulation for dynamic milling at small radial immersions. J Manuf Sci Eng-Trans ASME, 2003, 125(3): 416–422

11 Li Z, Liu Q. Solution and analysis of chatter stability for end milling in the time-domain. Chin J Aeronaut, 2008, 21(2): 169–178

12 Altintas Y, Budak E. Analytical prediction of stability lobes in milling. CIRP Ann-Manuf Technol, 1995, 44(1): 357–362

13 Budak E, Altintas Y. Analytical prediction of chatter stability in milling—Part I: General formulation. J Dyn Syst Meas Control-Trans ASME, 1998, 120(1): 22–30

14 Merdol S D, Altintas Y. Multi frequency solution of chatter stability for low immersion milling. J Manuf Sci Eng-Trans ASME, 2004, 126(3): 459–466

15 Altintas Y. Analytical prediction of three dimensional chatter stability in milling. JSME Int J Ser C-Mech Syst Mach Elem Manuf, 2001, 44(3): 717–723

16 Ko J H, Altintas Y. Dynamics and stability of plunge milling operations. J Manuf Sci Eng-Trans ASME, 2007, 129(1): 32–40

17 Kardes N, Altintas Y. Mechanics and dynamics of the circular milling process. J Manuf Sci Eng-Trans ASME, 2007, 129(1): 21–31

18 Ozturk E, Budak E. Dynamics and stability of five-axis ball-end milling. J Manuf Sci Eng-Trans ASME, 2010, 132(2): 021003

19 Bayly P V, Halley J E, Mann B P, et al. Stability of interrupted cutting by temporal finite element analysis. J Manuf Sci Eng-Trans ASME, 2003, 125(2): 220–225

20 Mann B P, Bayly P V, Davies M A, et al. Limit cycles, bifurcations, and accuracy of the milling process. J Sound Vibr, 2004, 277(1-2): 31–48

21 Mann B P, Young K A, Schmitz T L, et al. Simultaneous stability and surface location error predictions in milling. J Manuf Sci Eng-Trans ASME, 2005, 127(3): 446–453

22 Mann B P, Edes B T, Easley S J, et al. Chatter vibration and surface location error prediction for helical end mills. Int J Mach Tools Manuf, 2008, 48(3-4): 350–361

23 Insperger T, Stépán G. Semi-discretization method for delayed systems. Int J Numer Methods Eng, 2002, 55(5): 503–518

24 Insperger T, Stépán G. Updated semi-discretization method for periodic delay-differential equations with discrete delay. Int J Numer Methods Eng, 2004, 61(1): 117–141

25 Insperger T, Stépán G, Turi J. On the higher-order semi-discretizations for periodic delayed systems. J Sound Vibr, 2008, 313(1-2): 334–341

26 Insperger T, Mann B P, Stepan G, et al. Stability of up-milling and down-milling, Part 1: Alternative analytical methods. Int J Mach Tools Manuf, 2003, 43(1): 25–34

27 Mann B P, Insperger T, Bayly P V, et al. Stability of up-milling and down-milling, Part 2: Experimental verification. Int J Mach Tools Manuf, 2003, 43(1): 35–40

28 Long X H, Balachandran B, Mann B P. Dynamics of milling processes with variable time delays. Nonlinear Dyn, 2007, 47(1-3): 49–63

29 Long X H, Balachandran B. Stability analysis for milling process. Nonlinear Dyn, 2007, 49(3): 349–359

30 Sims N D, Mann B, Huyanan S. Analytical prediction of chatter stability for variable pitch and variable helix milling tools. J Sound Vibr, 2008, 317(3-5): 664–686

31 Seguy S, Insperger T, Arnaud L, et al. On the stability of high-speed milling with spindle speed variation. Int J Adv Manuf Technol, 2010, 48(9-12): 883–895

32 Wan M, Zhang W H, Dang J W, et al. A unified stability prediction method for milling process with multiple delays. Int J Mach Tools Manuf, 2010, 50(1): 29–41

33 Olgac N, Sipahi R. A unique methodology for chatter stability mapping in simultaneous machining. J Manuf Sci Eng-Trans ASME, 2005, 127(4): 791–800

34 Butcher E A, Ma H, Bueler E, et al. Stability of linear time-periodic delay-differential equations via chebyshev polynomials. Int J Numer Methods Eng, 2004, 59(7): 895–922

35 Butcher E A, Bobrenkov O A, Bueler E, et al. Analysis of milling stability by the chebyshev collocation method: Algorithm and optimal stable immersion levels. J Computat Nonlinear Dyn, 2009, 4(3): 031003

36 Ding Y, Zhu L, Zhang X, et al. A full-discretization method for prediction of milling stability. Int J Mach Tools Manuf, 2010, 50(5): 502–509

37 Ding Y, Zhu L, Zhang X, et al. On a Numerical method for simultaneous prediction of stability and surface location error in low radial immersion milling. J Dyn Syst Meas Control-Trans ASME, 2011, 133(2): 024503

38 Insperger T. Full-discretization and semi-discretization for milling stability prediction: Some comments. Int J Mach Tools Manuf, 2010, 50(7): 658–662

39 Ding Y, Zhu L, Zhang X, et al. Numerical integration method for prediction of milling stability. J Manuf Sci Eng-Trans ASME, 2011, 133(3): 031005

40 Ding Y, Zhu L, Zhang X, et al. Spectral method for prediction of chatter stability in low radial immersion milling. Proceedings-IEEE International Conference on Robotics and Automation, 2011, Shanghai, China. 4359–4363

41 Tang T, Xu X, Cheng J. On spectral methods for volterra integral equations and the convergence analysis. J Comput Math, 2008, 26(6): 825–837

42 Ali I, Brunner H, Tang T. Spectral methods for pantograph-type differential and integral equations with multiple delays. Frontiers Math China, 2009, 4(1): 49–61

43 Khasawneh F A, Mann B P. A Spectral Element Approach for the Stability of Delay Systems. Int J Numer Methods Eng, 2011, 87(6): 566–592

44 Trefethen L N. Spectral Methods in Matlab, Society for Industrial and Applied Mathematics, Philadelphia, 2000

45 Yang W Y, Cao W, Chung T S, et al. Applied Numerical Methods Using Matlab. Hoboken, N.J.: Wiley-Interscience, 2005

46 Berrut J P, Trefethen L N. Barycentric lagrange interpolation. SIAM Rev, 2004, 46(3): 501–517

47 Farkas M. Periodic Motions. New York: Springer-Verlag, 1994

48 Henninger C, Eberhard P. Improving the computational efficiency and accuracy of the semi-discretization method for periodic delay-differential equations. Eur J Mech A-Solids, 2008, 27(6): 975–985

49 Zhu L M, Ding H, Xiong Y L. Third-order point contact approach for five-axis sculptured surface machining using non-ball-end tools (I): Third-order approximation of tool envelope surface. Sci China Tech Sci, 2010, 53(7): 1904–1912

50 Zhu L M, Ding H, Xiong Y L. Third-order point contact approach for five-axis sculptured surface machining using non-ball-end tools (II): Tool positioning strategy. Sci China Tech Sci, 2010, 53(8): 2190–2197

51 Ye T, Xiong C H, Xiong Y L, et al. Kinematics constrained five-axis tool path planning for high material removal rate. Sci China Tech Sci, 2011, 54: 3155–3165

52 Mao X Y, Liu H Q, Li B. Time-frequency analysis and the detecting method research on the milling force token signal in the spindle current signal. Sci China Ser E-Tech Sci, 2009, 52: 2810–2813

53 Liu H Q, Chen Q H, Li B, et al. On-line chatter detection using servo motor current signal in turning. Sci China Tech Sci, 2011, 54: 3119–3129